American Journal of Electrical and Computer Engineering
2024, Vol. 8, No. 2, pp. 59-70
https://doi.org/10.11648/j.ajece.20240802.14

Research Article

Design and Analysis of an Adaptive Pipeline Detection and Correction Mechanism

Hongsheng Li[1], Xiaonan Zhao[1], Zhuli Zhang[1], Shutao Feng[2, *], Lei Jian[2], Gang Liu[2]

[1]Jingneng (Xilingol) Power Generation Co., Ltd, Xilingol League, China
[2]Beijing Energy Engineering Intelligent Robot Co., Ltd, Beijing, China

Abstract

This paper presents a novel adaptive pipeline probe detection and correction mechanism designed to address the challenge of detection interference caused by the movement of wall-climbing robots, particularly in complex environments such as water-cooled walls. The mechanism ensures that the detection probe can accurately detect individual pipelines even when the robot deviates from its intended path. To achieve this, the system incorporates a self-adaptive deviation correction mechanism that maintains consistent detection performance without requiring adjustments to the robot's spatial position. The design includes a variable stiffness analysis of the buffer spring within the correction mechanism, which is optimized to minimize the impact of the robot's movement on the detection components. By carefully selecting the spring's size and stiffness parameters, the mechanism reduces vibration and enhances the stability and reliability of pipeline detection under offset conditions. In addition to maintaining detection accuracy, the system also supports automatic marking of pipelines that exhibit quality issues, ensuring that any detected defects are easily traceable. This adaptive mechanism not only improves detection efficiency but also enhances the overall operational stability of wall-climbing robots in industrial inspection tasks. The results demonstrate the mechanism's effectiveness in mitigating the challenges posed by uneven friction and time delays in the control system, making it a significant contribution to the field of robotic inspection systems.

Keywords

Self-Adaptation, Rectification Mechanism, Spring Stiffness Analysis, Pipeline Inspection

1. Introduction

The detection of water-cooled wall pipelines is a critical task for wall-climbing robots used in industrial inspection, particularly within thermal power plants [1, 2]. These robots often utilize ultrasonic detection probes, such as those developed by Zero Sound Technology, which require a precise distance of approximately 2 mm between the probe and the pipeline for accurate detection. However, the complex geometry of water-cooled wall pipelines presents challenges, including varying friction forces due to changes in the number and area of magnets on either side of the robot as it traverses the wall. This uneven friction, coupled with time delays in the control system's correction mechanism, frequently causes the robot to deviate towards the side with less friction, thereby compromising detection accuracy [3].

*Corresponding author: Fst15801315085@163.com (Shutao Feng)

Received: 12 August 2024; **Accepted:** 5 September 2024; **Published:** 29 September 2024

Recent advancements in wall-climbing robot design have sought to address these challenges, focusing on improving adaptability, stability, and detection accuracy. Liu et al. [4] introduced a bio-inspired wall-climbing robot that enhances surface adaptability using spine wheels, adhesive belts, and eddy suction cups. This innovation is particularly relevant for robots operating on uneven and complex surfaces, as it ensures consistent detection performance. Jiang et al. [5] extended this research by analyzing the failure modes of rolling sealed robots, providing valuable insights into the reliability of these robots during operation, which is crucial for maintaining the integrity of inspection tasks.

Building on the need for reliable contact with complex surfaces, Wang et al. [6] examined the safe adsorption conditions necessary for stable robot operation. Their work highlights the importance of optimizing the robot's interaction with the wall to prevent deviations that could affect detection accuracy. Li et al. [7] furthered these advancements by developing a wheeled robot that employs bio-inspired dry adhesives, enhancing the robot's adherence and detection capabilities across diverse pipeline geometries. This development is instrumental in reducing errors caused by deviations during the robot's movement.

To complement these design improvements, Wang et al. [8] proposed a switching motion control strategy that enhances the robot's motion accuracy, even in the face of friction imbalances or other environmental factors. This control strategy is vital for ensuring that the robot can maintain precise detection under varying conditions, addressing one of the core challenges in the detection of water-cooled wall pipelines.

In light of these recent developments, it is evident that an adaptive pipeline detection and correction mechanism must be designed with a focus on both accuracy and stability [9]. Such a mechanism must prevent deviations during detection, ensure traceability of quality issues, and maintain the robot's stability by optimizing the center of gravity and reducing vibrations through the appropriate selection of spring stiffness. The following sections will outline the design considerations necessary to meet these requirements, ensuring the successful detection of pipelines by wall-climbing robots in industrial settings:

1) The detection mechanism must accommodate two detection probes simultaneously to enhance detection efficiency and enable cross-pipe detection without altering the robot's spatial position;
2) The detection probe must successfully complete the detection of a single pipeline even if the robot deviates during its movement;
3) The system should automatically mark any pipelines detected with quality issues to facilitate subsequent inspections;
4) The mechanism should be lightweight with a low center of gravity, and the selected spring stiffness should minimize vibrations.

This adaptive structure is therefore significant in improving the operational efficiency and accuracy of wall-climbing robots, particularly in challenging environments like water-cooled wall pipelines.

2. Scheme Design for Pipeline Detection and Rectification Mechanism

Based on the above design requirements, an adaptive pipeline detection and correction mechanism is designed in this paper. Its structure diagram is shown in Figure 1. It consists of a magnet and a detection probe. The detection device is fixed on the lifting slide table, and the distance between the probe and the pipeline can be adjusted. The main part of the detection device can slide on the self-adaptive correction guide rail, and an adaptive correction spring is placed at both ends of the detection device to reduce the impact on the correction mechanism during the deviation process of the climbing robot, and realize the detection mechanism without Automatic centering while working. The reversing steering gear can make the detection probe move along the reversing guide rail, and realize the detection across the pipeline without changing the spatial position of the robot, improving the detection efficiency.

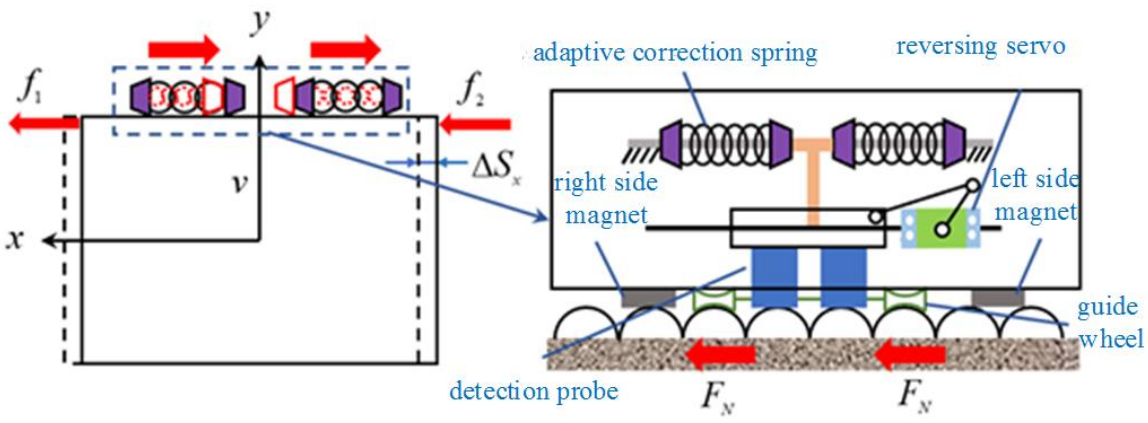

Figure 1. *Schematic diagram of the self-adaptive deviation correction detection mechanism of the wall-climbing robot.*

According to the design index of the wall-climbing robot and the specific parameters of each device, the weight of the detection mechanism of the upper load of the lifting slide table is 60N, and the sliding table module is selected for the lifting slide table. When the wall-climbing robot is running, the lifting slide table and the wall is vertical, so the value of the axial load F_a of the lead screw of the lifting slide table can be obtained by the following formula:

$$F_a = G_{total} + \mu mg \tag{1}$$

According to the design manual of the selected slide module, where

μ ——Friction coefficient between slider and screw $u = 0.1$;

m ——The total mass of slider and detection mechanism, take $m = 6.5Kg$;

G_{total} ——The total gravitational force.

Therefore, the value of the required drive torque T_a can be obtained from the following formula when the lifting slide is running at a constant speed

$$T_a = \frac{F_a p}{2\pi\eta} = 11.7\text{kgf} \cdot \text{cm} \tag{2}$$

According to the design manual of the selected slide module, where

p ——screw lead, $p = 10mm$;

η ——Lead screw feed efficiency, $\eta = 0.9$;

In order to reduce the space occupied by the electronic control components of the wall-climbing robot, the driving torque required by formula (2) is comprehensively considered, and finally the DS-R009B integrated steering gear is selected. Its detailed parameters are shown in Table 1, and the real object is shown in Figure 2 shown.

Table 1. *DS-R009B Servo parameter.*

Parameter	Value
Working voltage range	18V~28V
Rated voltage	24V
Rated torque	20kg/cm
Weight	302g
Operable angle	360 °±2 °
Mechanical limit angle	360 °

Figure 2. *DS-R009B steering gear physical map Stress Analysis and Design of Adaptive Correction Mechanism.*

3. Force Analysis and Design of Adaptive Correction Mechanism

Since the connection between the detection device in the adaptive correction mechanism and the reversing steering gear is a rigid connection, during the deviation correction process, there will be a certain impact on the reversing steering gear, and a compliant mechanism [10-13] is needed to realize the adaptive deviation correction For the reliable operation of the mechanism, in order to design reasonable mechanism parameters, it is necessary to establish the force balance equation of the probe support during the correction process of the adaptive correction mechanism and the relationship between the spring force and the blocking torque of the steering gear.

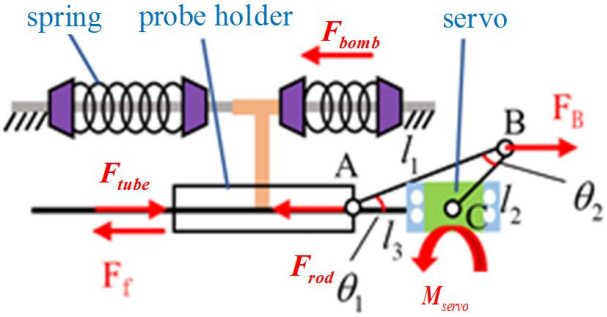

Figure 3. *The adaptive deviation correction mechanism moves to the right.*

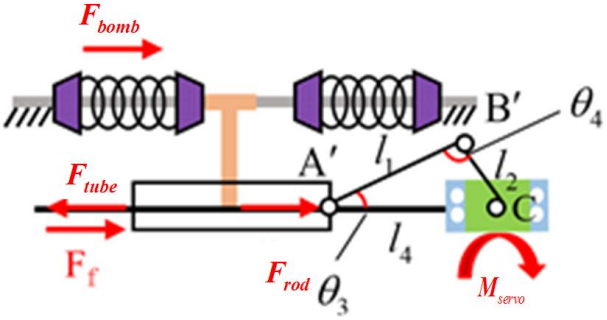

Figure 4. *The adaptive deviation correction mechanism moves to the left.*

Firstly, the mechanical analysis is carried out during the rightward movement of the correction mechanism. The probe support is subjected to the thrust F_{rod} of the rod, the lateral pressure F_{tube} of the pipeline and the friction force F_f of the guide rail, and the balance equation is established:

$$F_{rod} + F_f = F_{tube} \tag{3}$$

Since the steering gear has a certain stalling moment when it is powered on, and the fixed support of the steering gear is subjected to the elastic force of the spring and the force F_B exerted by the rod AB on the rod BC, the force balance equation is obtained:

$$\begin{cases} F_{bomb} = F_B \\ M_{rudder} = F_B + l_2 \end{cases} \tag{4}$$

Among them, the size of F_{bomb} is $K(x_0 - x)$, M_{rudder} is the locked-rotor torque of the steering gear, K is the spring stiffness, x_0 is the original length of the spring, and x is the length of the spring after deformation.

In order to prevent the deviation of the correction mechanism from causing damage to the steering gear, the resistance torque provided by the reverse buffer elastic force of the spring should be greater than the blocking torque of the steering gear, so the stiffness of the spring should meet the following conditions:

$$K \geq \frac{M_{rudder}}{(x_0 - x)l_2} \tag{5}$$

4. Finite Element Analysis of Adaptive Correction Spring

The spring is an important part of the self-adaptive pipeline detection and correction mechanism. The appropriate spring stiffness can ensure the correction performance of the mechanism, reduce the impact of the mechanism on the steering gear, and reduce the vibration frequency of the mechanism to improve the accuracy of probe detection. Therefore, for the self-adaptive correction spring Theoretical calculation of the stiffness and stress value of the spring, and the use of finite element analysis to check the stress and strength of the spring, so that the spring strength can meet the requirements, realize self-adaptive correction and impact resistance, and reduce the vibration frequency of the mechanism.

4.1. Theoretical Calculation of Spring Stiffness

The calculation formula of vertical stiffness of cylindrical coil spring is [14, 15]:

$$K = \frac{Gd^4}{8D^3 n} \tag{6}$$

In the formula G ——The shear modulus of the spring material, GPa;

d ——The diameter of the spring wire, mm;

D ——Spring diameter, mm;

n ——Number of coils.

4.2. Calculation of Vibration Frequency of Spring

In order to obtain a suitable spring stiffness to reduce the vibration frequency of the whole mechanism, the undamped free vibration equation of the spring system is established:

$$m\ddot{x} = -Kx \tag{7}$$

Where x is the distance between the balance position of the spring and the current position, m is the mass of the spring, so that the natural frequency $\omega_n = \sqrt{K/m}$, change the above formula to:

$$\ddot{x} + \omega_n^2 x = 0 \tag{8}$$

According to the general solution of the differential equation, we know that:

$$x = A\cos(\omega_n t - \varphi) \tag{9}$$

A is the amplitude, so the vibration frequency of the spring is:

$$f = \sqrt{\frac{K}{4m\pi^2}} \tag{10}$$

Therefore, in order to reduce the influence of the vibration of the spring system on the sampling frequency of the probe as much as possible, the stiffness coefficient of the spring should meet the following conditions:

$$K \leq f_m^2 4m\pi^2 \tag{11}$$

Among them, f_m is the frequency at which the probe uploads data to the host computer, and the frequency is 1 time per second. In the comprehensive formula (5), the range of the stiffness coefficient of the spring is:

$$\frac{M_{rudder}}{(x_0 - x)l_2} \leq K \leq f_m^2 4m\pi^2 \tag{12}$$

When the reversing steering gear is working, it is necessary

to drive the probe to detect the tube change, and there will be certain vibration during the reversing process. To reduce the weight of the adaptive correction mechanism, the size and weight of the steering gear should be as small as possible. Several common small servo parameters are shown in Table 2:

Table 2. *Common Small Servo Parameters.*

Type	Weight	Size	Maximum Working Torque
MG90	10g	32.5x22.5x12.5mm	2 kg cm
MG995	55g	40.7x19.7x42.9mm	13 kg cm
DS3225	60g	40x20x37.2mm	24.5 kg cm
SG90	9g	32x30x12.5mm	1.6 kg cm

It can be seen from Table 2 that the maximum working torque of DS3225 steering gear is better than that of other steering gears when the size and weight are small. Therefore, DS3225 servo steering gear is selected. Its technical parameters are shown in Table 3. The actual product is shown in the figure 5. The connecting rod BC is a model connecting rod with a length of $l_2 = 70mm$. When the control system actively corrects the deviation, the moving distance of the spring is 20mm, so the maximum value of $x_0 - x$ is 20mm, and the stiffness coefficient K of the spring is $1470N \cdot m^{-1}$.

Table 3. *DS3225 servo technical parameters.*

Parameters	Value
Working voltage range	4.8V~8.4V
Stall Torque	21kg cm~24.5kg cm
Stall current	1.9A~2.3A

Figure 5. *The physical picture of the reversing steering gear.*

4.3. Spring Stiffness Design and Finite Element Analysis

Using finite element analysis, the spring model is established, and flat cylinders are added at both ends of the spring as the fixed end and force end of the spring force finite element analysis. The force application position is shown in Figure 6:

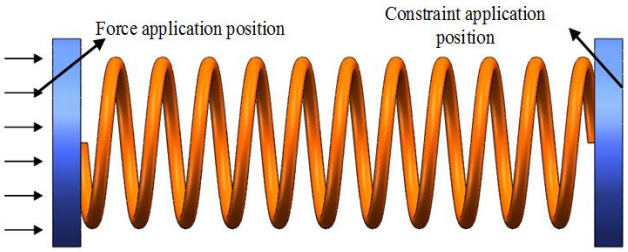

Figure 6. *Schematic diagram of spring simulation fixation and force application position.*

To analyze the influence of the spring model parameters on the spring stiffness, the spring model selects a constant pitch spring, and the commonly used spring materials and corresponding physical parameters are shown in Table 4:

Table 4. *Physical parameters and scope of application of common spring materials.*

Standard number	Spring grade	Shear modulus (GPa)	Suitable temperature (℃)	Applicable scope
GB4357	70Mn	79000	-40~130	Low, medium and high tension springs
GB4358	T8MnA	79000	-40~130	valve spring
GB4359	65Mn70	79000	-40~150	Internal combustion engine valve spring
GB4360	65Mn	79000	-40~150	General Machinery Springs
GB4361	60Si2MnA	79000	-40~200	high load spring
GB4362	55CrSi	79000	-40~250	High temperature high stress spring

Since 65Mn spring steel has high strength after heat treatment and cold drawing hardening, it has certain flexibility and plasticity, and is mainly used for small-sized general mechanical springs. Therefore, the spring material of the self-adaptive correction mechanism designed in this paper uses 65Mn carbon Structural steel, for the influence of different variables on the spring stiffness, the control variable method is used, and Solid Works is used for finite element analysis.

The essence of finite element analysis is to first discretize the continuous object into a discrete body with a finite number of units connected to each other through nodes [16-19], and use the interpolation formula to establish the displacement of the unit

$$\{f\}=[N]\{\delta\}^E \tag{13}$$

Where $[N]$ is the shape function matrix, $\{\sigma\}^e$ is the unit node displacement, and the above formula is substituted into the geometric equation

$$\{\sigma\}=[\partial]\{f\}=[\partial][N]\{\sigma\}^e=[B]\{\sigma\}^e \tag{14}$$

$$\{\varepsilon\}=[\partial]\{f\}=[\partial][N]\{\sigma\}^e \tag{15}$$

where $[B]$ is the strain transformation matrix, and $[\partial]$ is represented in the space as

$$[\partial]=\begin{bmatrix} \frac{\partial}{\partial x} & 0 & 0 \\ 0 & \frac{\partial}{\partial y} & 0 \\ 0 & 0 & \frac{\partial}{\partial z} \\ \frac{\partial}{\partial y} & \frac{\partial}{\partial x} & 0 \\ 0 & \frac{\partial}{\partial z} & \frac{\partial}{\partial y} \\ \frac{\partial}{\partial z} & 0 & \frac{\partial}{\partial x} \end{bmatrix} \tag{16}$$

Using the stress transformation matrix $[S]=[D][B]$, where $[D]$ is the elasticity matrix

$$[D][B]\{\sigma\}^e=[s]\{\sigma\}^e \tag{17}$$

$$[D]=\begin{bmatrix} \frac{E(1-\mu)}{(1+\mu)(1-2\mu)} & \frac{E\mu}{(1+\mu)(1-2\mu)} & \frac{E\mu}{(1+\mu)(1-2\mu)} & 0 & 0 & 0 \\ \frac{E\mu}{(1+\mu)(1-2\mu)} & \frac{E(1-\mu)}{(1+\mu)(1-2\mu)} & \frac{E\mu}{(1+\mu)(1-2\mu)} & 0 & 0 & 0 \\ \frac{E\mu}{(1+\mu)(1-2\mu)} & \frac{E\mu}{(1+\mu)(1-2\mu)} & \frac{E(1-\mu)}{(1+\mu)(1-2\mu)} & 0 & 0 & 0 \\ 0 & 0 & 0 & \frac{E\mu}{2(1+\mu)} & 0 & 0 \\ 0 & 0 & 0 & 0 & \frac{E\mu}{2(1+\mu)} & 0 \\ 0 & 0 & 0 & 0 & 0 & \frac{E\mu}{2(1+\mu)} \end{bmatrix} \tag{18}$$

where E is the modulus of elasticity and μ is Poisson's ratio.

Using the principle of virtual work, the stress of subdivided elements can be obtained

$$\{F\}^e=\iiint_{V^e}[B]^T[D]dxdydz\{\sigma\}^e=[k]^e\{\sigma\}^e \tag{19}$$

where $[K]^e$ is the stiffness matrix.

The total potential energy of the overall discretized structure is

$$\sum_{e=1}^{ne}\prod{}_p^e=\sum_{e=1}^{ne}U^e+\sum_{e=1}^{ne}V^e \tag{20}$$

Among them, V^e is the potential energy of external force, U^e is the potential energy of deformation, and the displacement of the node can be substituted into

$$\prod{}_p=\sum_{e=1}^{ne}\frac{1}{2}\{\sigma\}^T[K]\{\sigma\}-\sum_{e=1}^{ne}\{\sigma\}^T\{R\}^e \tag{21}$$

Based on the above formula, the finite element method is based on the principle of energy. It solves the displacement for each unit of the discretized structure, and then obtains the stress and strain of the unit. Therefore, as long as the units are divided, the calculation can be performed using a general-purpose computer program.

According to the common spring size parameters on the market, first select the middle diameter of 6mm, the number of effective turns of 8 turns, and the pitch of 5mm to analyze the relationship between the spring wire diameter and stiffness. Because too small spring wire diameter will lead to excessive spring deformation, Solid Works will use the display method of large displacement flag, this method is unreliable, and it is easy to cause the solver error to cause the simulation analysis to fail, so from the wire diameter of 0.4 mm to start the analysis, gradually increase the diameter of the spring wire, and find out the relationship between the diameter of the spring wire and the stiffness.

Table 5. *Relationship between spring wire diameter and stiffness.*

D (mm)	0.4	0.5	0.6	0.7	0.8	1.0
K (N m^{-1})	144	347	682	1443	2513	5429

Since the required minimum spring stiffness is $1470N \cdot m^{-1}$, keep the spring wire diameter 0.8 mm unchanged, gradually increase the spring diameter, and analyze the relationship between the spring diameter and stiffness. The middle diameter of the spring is 6mm, and the number of effective turns is 8. In order to avoid the error reported by the solver caused by the excessive deformation of the spring caused by the excessive force applied, and because the stiffness of the spring is constant under the given spring structure parameters, the applied external force is set. is 0.01N. When the pitch is 5mm and the wire diameter is 0.8mm, the deformation of 0.01N force is shown in Figure 7:

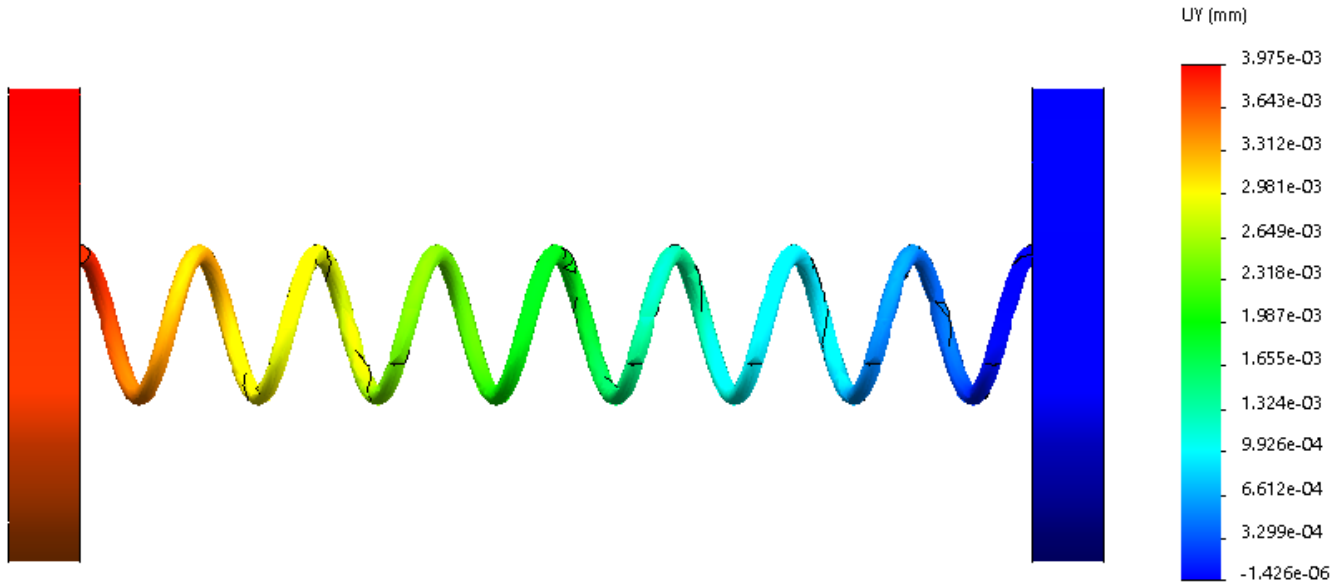

Figure 7. *Cloud diagram of spring deformation with optimal spring wire diameter.*

Table 6. *Relationship between spring pitch diameter and stiffness.*

d (mm)	6	7	8	9	10	11
K (N m^{-1})	2513	1585	963	668	474	377

It can be seen from Table 6 that the spring diameter is 7 mm to meet the requirements, and finally keep the spring wire diameter of 0.8 mm and the spring diameter of 7 mm unchanged, continuously increase the number of spring coils, and analyze the relationship between the number of spring coils and the stiffness. The middle diameter of the spring is 7mm, the number of effective turns is 8, the pitch is 5mm, and the wire diameter is 0.8mm, the deformation of which is applied with a force of 0.01N is shown in Figure 8:

Table 7. *The relationship between the number of spring coils and stiffness.*

Laps (n)	8	9	10	11	12	13
K (N m^{-1})	1585	1428	1250	1129	1004	937

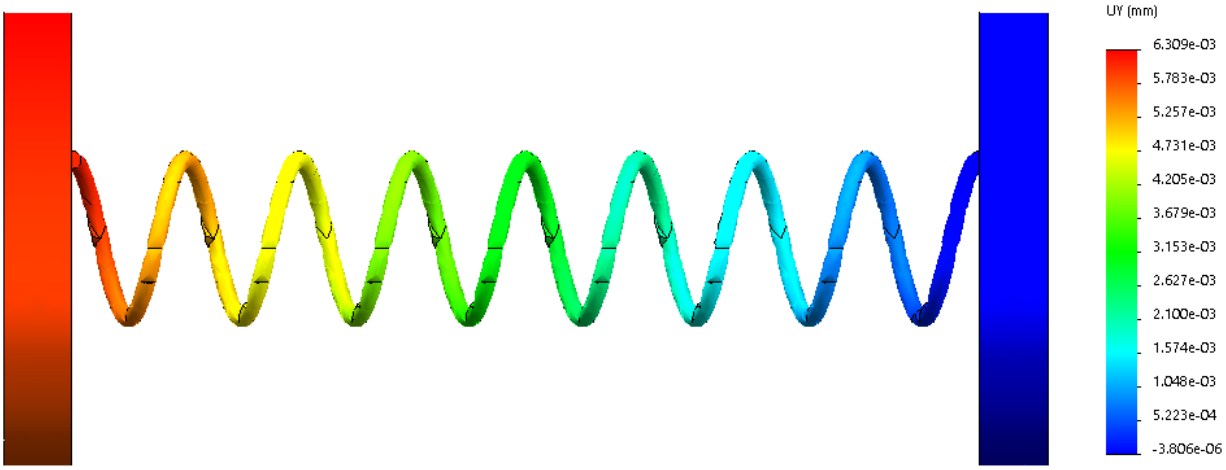

Figure 8. *Cloud diagram of spring deformation with optimal spring pitch diameter.*

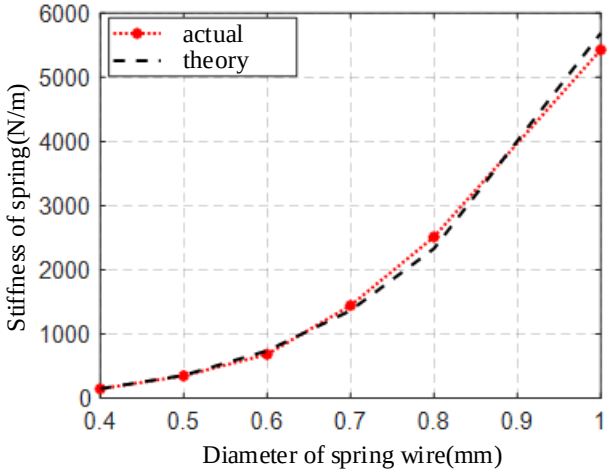

Figure 9. *Relationship between spring wire diameter and spring stiffness.*

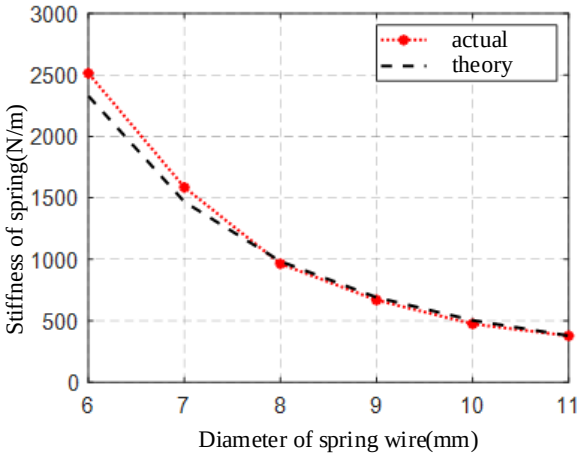

Figure 10. *Relationship between spring pitch diameter and spring stiffness.*

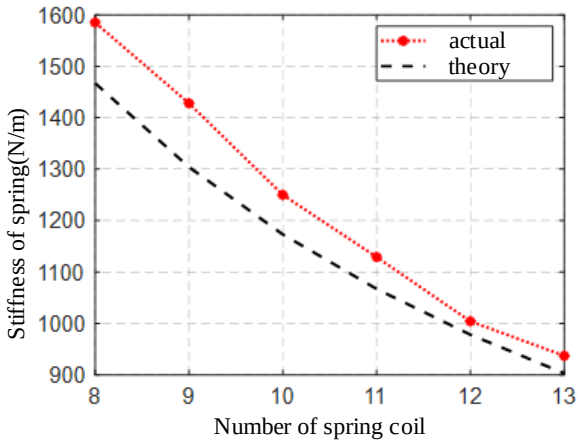

Figure 11. *The relationship between the number of coils and spring stiffness.*

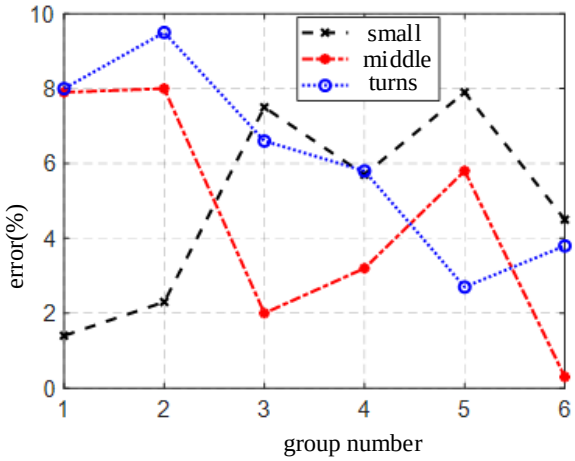

Figure 12. *Error values of different spring parameters.*

From the theoretical calculation formula of spring stiffness and Tables 5 to 7, the relationship between the theoretical

values and simulation values of different parameters and stiffness of springs can be obtained, as shown in Figures 9 to 11. The simulation values of spring stiffness and the theoretical calculation of stiffness should have an error within 10%. According to the error value data shown in Figure 12, the simulation results have certain reliability.

According to the required minimum spring stiffness $1470N \cdot m^{-1}$ and the data of the simulation results, a 65Mn spring with a spring wire diameter of 0.8mm, a middle diameter of the spring of 7mm, and a number of coils of 8 is finally selected.

For a general structure, its motion can be synthesized by its free vibration mode, so the modal analysis of finite element is used to verify the influence of the selected spring vibration on the sampling frequency of the probe. Since the impact of the spring vibration on the probe is mainly along the forward direction of the wall-climbing robot and in the direction perpendicular to it, the modes corresponding to the vibration in these two directions, namely the fourth-order and first-order modes, are analyzed, as shown in the figures 13~14 shown.

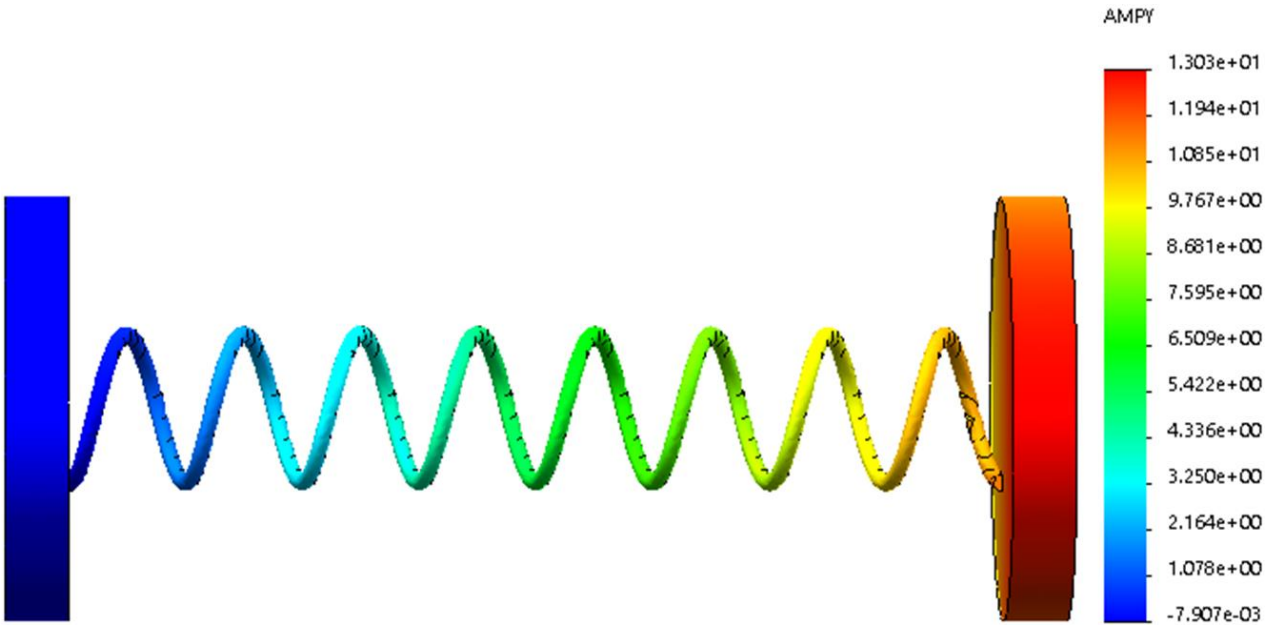

Figure 13. *The fourth-order mode diagram of the spring.*

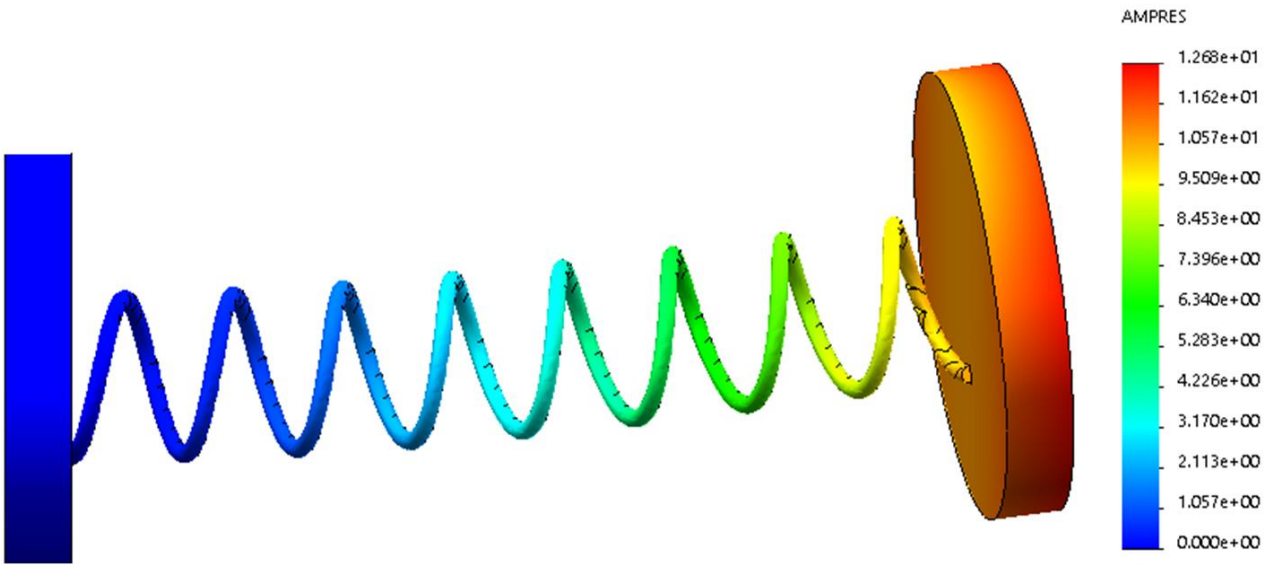

Figure 14. *The first-order mode diagram of the spring.*

According to Figures 13~14, it can be seen that the vibration frequency of the spring is much smaller than the sampling frequency of the probe, and the influence on the sampling of the probe can be ignored.

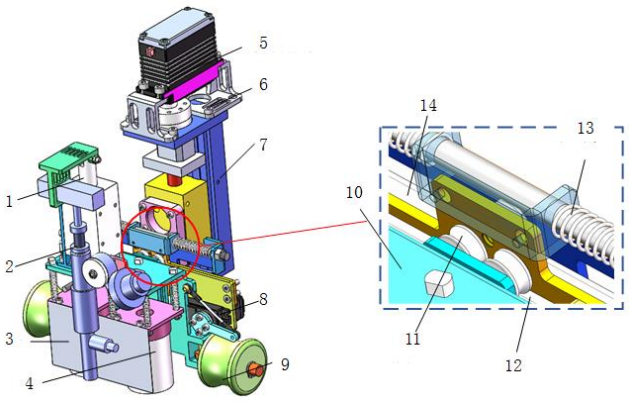

Figure 15. *Three-dimensional model of the self-adaptive deviation correction detection mechanism of the wall-climbing robot (1. electromagnet 2. spraying device 3. spray baffle 4. detection probe 5. Lifting steering gear 6. Steering gear support 7. Lifting and lifting platform8. Reversing steering gear 9. Guide wheel 10. Support for probe11. The pulley 12. Reversing guide rail 13. Self-adapting offset spring14. Adaptive deviation correcting guide).*

According to the spring parameters selected in the design calculation, the three-dimensional model of the adaptive pipeline detection and correction mechanism is established. In order to reduce the weight and center of gravity of the adaptive correction mechanism, the minimum stroke of 20mm is selected for the slide table, and the steering gear bracket and the probe support are sampled from aluminum alloy. material, and there are multiple weight-reducing process holes in the non-load-bearing position, and the quality-punched detection probe and spraying device are placed at the bottom of the deviation-correcting mechanism to lower the center of mass of the overall mechanism, as shown in Figure 15. A spraying device is placed on the upper end of the detection probe, which is driven by an electromagnet. When the detection probe detects that the pipeline is abnormal, it will send a driving signal to the electromagnet to realize the automatic marking function of spraying. At the same time, there is a spraying baffle at the front of the probe. In order to avoid the impact of spray paint on the probe. The guide wheels are attached to the pipe, and each probe is placed directly above the pipe. When the body of the wall-climbing robot deviates, the probe and the spraying device move along the self-adaptive correction guide rail, and the self-adaptive correction spring is compressed, and the spring acts as a buffer. When the detection device needs to perform tube replacement detection, the lifting steering gear raises the probe, and the reversing steering gear drives the connecting rod to move the probe along the reversing guide rail to realize tube replacement detection.

The self-adaptive pipeline correction mechanism designed in this paper is mainly applied to the curved surface pipeline detection of the water wall of the boiler power station, which effectively solves the problems of high risk and low accuracy of manual detection caused by the complexity of the curved surface environment; In case of deviation during the inspection process, a passively adjusted spring is added to the detection part of the probe, and at the same time, the coverage area of the detection device is increased by cooperating with the reversing steering gear.

5. Performance Test of Adaptive Pipeline Detection and Correction Mechanism

Due to the dark light on the inner wall of the boiler, the movement of the deviation correction mechanism is not obvious. Therefore, the performance test of the deviation correction mechanism is carried out by using the water wall test frame built outside the boiler. The actual operation effect is shown in Figure 16:

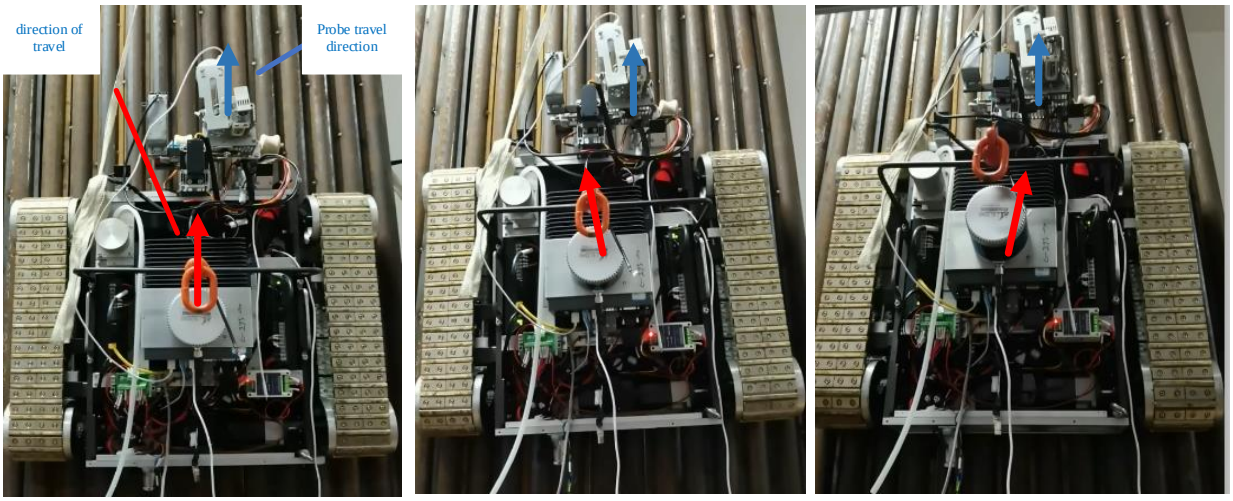

(a) (b) (c)

Figure 16. *Operation experiment of adaptive pipeline detection and correction mechanism: (a) The body moves straight up; (b) The body shifts to the left; (c) The body shifts to the left.*

It can be seen from the figure that when the vehicle body deviates left and right, the detection device is always directly above the pipeline due to the existence of the adaptive pipeline detection and correction mechanism.

6. Conclusions

In this paper, the mechanism design and analysis of the detection requirements of water-cooled pipes are carried out. The main achievements are divided into the following parts:

1) A pipeline probe detection mechanism with self-adaptive correction is proposed, which realizes the stability and accuracy of the pipeline detection probe during the operation of the wall-climbing robot;
2) Based on the theory of passive compliance, the stiffness of the spring of the self-adaptive correction mechanism is analyzed, and the maximum stall torque of the steering gear is used as the limiting condition, and the influence of the wire diameter, pitch diameter and number of turns of the spring on the stiffness is analyzed. The error of the result is less than 10%, which has certain reliability;
3) The pipeline probe detection mechanism with adaptive deviation correction reduces the impact of the adaptive deviation correction mechanism on the reversing steering gear during the offset process, and reduces the impact on the detection accuracy of the pipeline probe caused by the free vibration of the spring.

Conflicts of Interest

The authors declare no conflicts of interest.

References

[1] Jiang Ze, Chen Bo, Ju Zhongjin, Li Yichao, Xu Yundou, Zhao Yongsheng. Design and analysis of a wall-climbing robot for water wall inspection of thermal power plants [J]. Journal of Field Robotics, 2023, 40(5): 1003-1013. https://doi.org/10.1002/rob.22171

[2] Zhu Shiqiang, Gao Zhenfei, Song Wei, etc. Research on dynamic modeling of wall-climbing robot over welding process [J]. Journal of Agricultural Machinery, 2020, 51(12): 377-383. https://doi.org/10.6041/j.issn.1000-1298.2020.12.041

[3] Gui Zhongcheng, Chen Qiang, Sun Zhenguo. Multi-body flexible permanent magnetic adsorption wall-climbing robot [J]. Chinese Journal of Mechanical Engineering, 2008, 44(6): 177-182. https://doi.org/10.3321/j.issn:0577-6686.2008.06.027

[4] Liu Jinfu, Xu Linsen, Chen Shouqi, etc. Development of a bio-inspired wall-climbing robot composed of spine wheels, adhesive belts and eddy suction cup [J]. Robotica, 2021, 39(1): 3-22. https://doi.org/10.1017/S026357471900184X

[5] Liu Zhihui, Cai Wei, Fu Xingwei, etc. Failure Analysis of a Rolling Sealed Wall Climbing Robots [J]. China Mechanical Engineering, 2022, 33(22): 2755. https://doi.org/10.3969/j.issn.1004-132X.2022.22.014

[6] Jang Dezheng, Hu Jun, Zhong Heng, etc. Analysis of Safe Adsorption Conditions and Motion Characteristics of Rolling Sealed Tracked Wall-climbing Robot [J]. China Mechanical Engineering, 2021, 32(22). https://doi.org/10.3969/j.issn.1004-132X.2021.22.013

[7] Li Hongkai, Sun Xianfei, Chen Zishuo, etc. Design of a wheeled wall climbing robot based on the performance of bio-inspired dry adhesive material [J]. Robotica, 2022, 40(3): 611-624. https://doi.org/10.1017/S0263574721000710

[8] Wang Congqing, Gu Jiayue, Li Zhiyu. Switching motion control of the climbing robot for aircraft skin inspection [C] //2019 IEEE International Conference on Fuzzy Systems (FUZZ-IEEE). IEEE, 2019: 1-6. https://doi.org/10.1109/FUZZ-IEEE.2019.8858987

[9] Wang Yang, Zhang Xiaojun, Zhang Minglu, etc. Design and analysis of a split flexible wall-climbing robot that can adapt to variable curvature facades [J]. Chinese Journal of Mechanical Engineering, 2021, 57(3): 49-58. https://doi.org/10.3901/JME.2021.03.049

[10] Jiang Junxia, Zhang Xinyuan, Tao Bangming, etc. Design and experiment of motor teleoperation replacement mechanism based on passive compliance mechanism [J]. Journal of Zhejiang University, 2021, 55(05): 855-865+886. https://link.cnki.net/urlid/33.1245.T.20210531.0940.010

[11] Mu Zaile. Research on Compliant Control of Upper and Lower Limb Rehabilitation Robots [D]. Wuxi: Jiangnan University, 2020. https://doi.org/10.27169/d.cnki.gwqgu.2020.000561

[12] Huang Ting. Research on robot polishing method based on passive compliance control [D]. Suzhou: Soochow University, 2017. https://doi.org/CNKI:CDMD:1.1018.016653

[13] Yan Wen, Huang Yumei, Lin Wenzhou, etc. A force-position control method for plane grinding with passive compliance control [J]. Machinery Science and Technology, 2019, 38(06): 892-896. https://doi.org/10.13433/j.cnki.1003-8728.20190049

[14] Lin Binghong, Huang Zhihui, Wang Yuhui, etc. Stiffness and stress analysis of special-shaped car seat springs [J]. Journal of Huaqiao University, 2021, 42(06): 720-724.

[15] General Administration of Quality Supervision, Inspection and Quarantine of the People's Republic of China, National Standardization Management Committee. Design calculation of cylindrical helical spring: GB/T 23935-2009 [S]. Beijing: China Standard Press, 2009.

[16] Liu Dongying. Research on Computational Theory of Composite Truss Based on Finite Element Analysis [D]. Hefei: Hefei University of Technology, 2005. https://doi.org/10.7666/d.y747122

[17] Ning Lianwang. ANSYS Finite Element Analysis Theory and Development [J]. Shanxi Science and Technology, 2008(04): 65-66+68. https://doi.org/10.3969/j.issn.1004-6429.2008.04.035

[18] Cao Yanyan, Zhao Dengfeng. Finite Element Modal Analysis Theory and Its Application [J]. Mechanical Engineering and Automation, 2007(01): 73-74. https://doi.org/10.3969/j.issn.1672-6413.2007.01.027

[19] Han Song. Theoretical research on plane equivalent truss model based on finite element method [D]. Changsha: Hunan University, 2007. https://doi.org/10.7666/d.d031304